

# Characterization of Tribological and Mechanical Properties of the Si<sub>3</sub>N<sub>4</sub> Coating Fabricated by Duplex Surface Treatment of Pack Siliconizing and Plasma Nitriding on AISI D2 Tool Steel



MOJTABA NAJAFIZADEH, MEHRAN GHASEMPOUR-MOUZIRAJI,  
BEHZAD SADEGHI, and PASQUALE CAVALIERE

Silicon nitride (Si<sub>3</sub>N<sub>4</sub>) coating was deposited on AISI D2 tool steel through employing duplex surface treatments—pack siliconizing followed by plasma nitriding. Pack cementation was performed at 650 °C, 800 °C, and 950 °C for 2 and 3 hours by using various mixtures to realize the silicon coating. X-ray diffraction analyses and scanning electron microscopy observations were employed for demonstrating the optimal process conditions leading to high coating adhesion, uniform thickness, and composition. The optimized conditions belonging to siliconizing were employed to produce samples to be further processed via plasma nitriding. This treatment was performed with a gas mixture of 75 pct H<sub>2</sub>-25 pct N<sub>2</sub>, at the temperature of 550 °C for 7 hours. The results showed that different nitride phases such as Si<sub>3</sub>N<sub>4</sub>-β, Si<sub>3</sub>N<sub>4</sub>-γ, Fe<sub>4</sub>N, and Fe<sub>3</sub>N can be recognized as coatings reinforcements. It was demonstrated that the described composite coating procedure allowed to obtain a remarkable increase in hardness (80 pct higher with respect to the substrate) and wear resistance (30 pct decrease of weight loss) of the tool steel.

<https://doi.org/10.1007/s11661-021-06410-6>  
© The Author(s) 2021

## I. INTRODUCTION

THE D-type is high carbon (1.4 to 1.6 wt pct) and high chromium (11 to 13 wt pct) tool steels. They are characterized by very high strength and mechanical stability at elevated temperature, high hardness, good corrosion, and wear resistance. The D2 tool steel is mainly employed for cold extrusion dies production.<sup>[1–4]</sup> Obviously, their surface properties are normally improved through simple or complex case hardening processes. As a matter of fact, surface properties are

mainly improved through intermetallics precipitation that can shift the main wear mechanisms from an abrasive to an adhesive behavior. This avoids surface brittleness that can lead to crack formation.<sup>[5]</sup> In this view, pack hardening is demonstrated to effectively improve surface properties of the AISI D2 tool steel.<sup>[6]</sup> The halide activated pack cementation (HAPC) method is widely used for improving surface properties of metals and alloys.<sup>[7,8]</sup> During HAPC, powders at high temperature react with the halide activators in order to form vapor of the coating compounds during the reaction with the substrate. The HAPC method enables the fabrication of metallurgical coating with good adhesion to the metallic substrate and effective coating thickness.<sup>[9]</sup> HAPC silicides coatings have been successfully deposited over numerous materials such as Ni, V, Fe, and Ti-based alloys.<sup>[10–13]</sup> Additional elements are added to the coatings for improving the intrinsic mechanical properties through complex hard compounds precipitation.<sup>[8,14]</sup> The coatings performances improve through further processing such as plasma nitriding.<sup>[1,15,16]</sup> Recently, siliconized layers deposited on AISI steels showed high wear and good pitting corrosion resistance. These improvements were attributed to the formation of hard FeSi intermetallic compounds.<sup>[17]</sup> The precise control of the optimal precipitation is demonstrated to be very beneficial for the corrosion resistance.<sup>[18]</sup> The

---

MOJTABA NAJAFIZADEH is with the School of Materials Science and Engineering, Shanghai Jiao Tong University, Shanghai, 200240, China. MEHRAN GHASEMPOUR-MOUZIRAJI is with the Group - Emerging: Materials, Research, Technology, School of Design, Management and Production Technologies, University of Aveiro, Estrada do Cercal 449, 3720-509 Oliveira de Azeméis, Portugal and also with the TEMA - Centre for Mechanical Technology and Automation, University of Aveiro, Aveiro, Portugal. BEHZAD SADEGHI is the Centre of Excellence for Advanced Materials Application, Slovak Academy of Sciences, Dubravská Cesta 9, 84511, Bratislava, Slovak Republic. PASQUALE CAVALIERE is with the Department of Innovation Engineering, University of Salento, Via per Arnesano, 73100, Lecce, Italy. Contact e-mail: [pasquale.cavaliere@unisalento.it](mailto:pasquale.cavaliere@unisalento.it)

Manuscript submitted May 18, 2021; accepted July 21, 2021.

two-step coating, based on the continual diffusion of two or more elements into the surface of the substrate, is demonstrated to be more and more effective.<sup>[19–22]</sup> Two-step coating technique, including diffusion of Ti,<sup>[23]</sup> Cr,<sup>[24]</sup> Al,<sup>[20]</sup> or B,<sup>[23]</sup> allows for the formation of hard nitrides. The nitride layers can modify the wear,<sup>[8,13]</sup> oxidation,<sup>[11]</sup> corrosion resistance,<sup>[12]</sup> and load-bearing capacity to very extreme levels. From an industrial point of view, pack cementation technique results simple, cost effective, and suitable for mass production for coating complex geometry substrates.<sup>[24–27]</sup>

The present study focused on the production and characterization of Si<sub>3</sub>N<sub>4</sub> coating on AISI D2 tool steel through a duplex treatment via pack siliconizing followed by plasma nitriding. First, optimized siliconizing coatings at high and low temperature were obtained. Then they were plasma nitrided in order to induce high strength and high wear resistance in the D2 steel.

## II. EXPERIMENTAL PROCEDURE

The substrate material is AISI D2 steel. The steel composition is listed in Table I (measured with Thermo Scientific ARL 3460 Advantage spectrometer).

For the HAPC, three types of powders containing different amounts of Si, NH<sub>4</sub>Cl (as a halide activator) with or without NaF, and Al<sub>2</sub>O<sub>3</sub> (as filler) were used. The composition of pack mixtures is listed in Table II.

For all the powders, Si is the donor source, NH<sub>4</sub>Cl or NH<sub>4</sub>Cl + NaF are employed as chemical activator, and Al<sub>2</sub>O<sub>3</sub> is employed as inert filler. Cylindrical steel samples (30\*30 mm) were cut and polished with metallographic SiC papers up to 600 finishing. Then, the specimens were cleaned with acetone and dried for further coating operations. Cubic stainless steel boxes with dimensions of 100\*100\*100 mm were half filled with the powder mixture and, after that the three steel samples were positioned on the mixture, the boxes were completely filled with the remaining powders. The samples were heated into a furnace (Hefei Kejing Material Technology Company, model KSL-1400X) at 650 °C, 800 °C, and 950 °C for 2 and 3 hours. After HAPC, the samples were polished via standard metallographic techniques for microscopy observations performed by employing a ZEISS EVO 40 scanning electron microscope equipped with EDS, the working distance was 10 mm, and the accelerating voltage was 20 kV.

The samples selected for further processing were those experiencing the best adhesion, thickness, and hardness. The plasma nitriding was performed by employing a gas blend of 75 pct H<sub>2</sub>-25 pct N<sub>2</sub> at 550 °C for 7 hours under a constant pressure of 10 mbar with a voltage applied between anode and cathode lying in the range of 300 to 800 volts. After 7 hours nitriding, the specimens were slowly cooled to 170 °C before removal from the reaction chamber. For investigating the coatings phase composition, samples were analyzed through X-ray diffraction analyses (XRD)

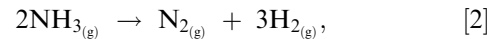
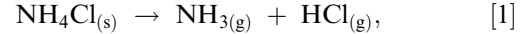
with a Rigaku diffractometer by applying Cu-K $\alpha$  radiation at a precipitating voltage of 40 kV and a current of 40 mA with a scan step of 0.02. For tribological studies, a pin-on-disk tribometer, under sideway slippage in dry conditions over a slippage distance of 500 m with a speed of 0.5 m/s under a vertical load of 30N (3 tests per condition were performed), was used. The specimens were prepared according to ASTM wear testing following the G99–04a standard. The material of the pin was tungsten carbide, and the disks were the specimens with coating and without coating. The wear weight loss after each 100m to 500m was calculated for each disk with an accuracy of 0.1 mg. The nano-mechanical properties of the coatings were studied through an Anton Paar nano-indenter model TTX-NHT2, equipped with a Berkovich diamond indenter. The tests were performed under loading control, with maximum applied load of 10 mN, loading and unloading rate of 20 mN/min, and dwell time of 5 s. Eleven indentations per sample were performed, and the average values were recorded. Hardness and elastic modulus were calculated by Oliver and Pharr method on the indentation load versus depth curves.

## III. RESULTS AND DISCUSSION

### A. Mechanism of Coatings

#### 1. Siliconizing coating

During the pack-siliconizing process, the chemical reactions taking place are described by Eqs. [1] through [10]. In the charge,<sup>[28]</sup>



On the substrate,

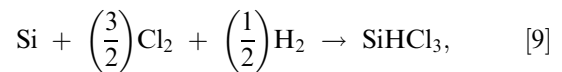
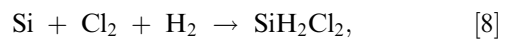
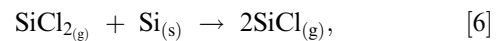
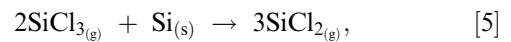
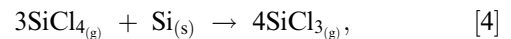


**Table I. Chemical Composition of the AISI D2 Tool Steel**

Element	Fe	C	Si	Mn	P	S	Cr	Mo	Ni	Cu	V
Composition (Wt Pct)	85	1.43	0.198	0.308	0.012	0.0075	12	0.8	0.0304	0.0901	0.124

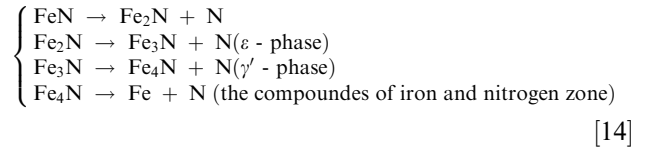
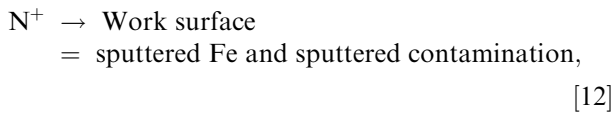
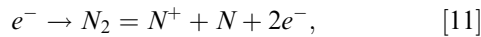
**Table II. Chemical Composition of Pack Mixtures, Time, and Temperature of the Pack Treatment**

Pack	Powder Composition (Wt Pct)				Time (h)	Temperature (°C)	Coded Value
	Si	NH <sub>4</sub> Cl	NaF	Al <sub>2</sub> O <sub>3</sub>			
1	12	0.5	—	87.5	2	650	12
						800	
						950	
2	12	0.5	0.5	87	3	650	13
						800	
						950	
3	10	0.5	0.5	89	2	650	32
						800	
						950	
3	10	0.5	0.5	89	3	650	33
						800	
						950	

During the siliconizing procedure, NH<sub>4</sub>Cl is the halide activator; the halide evaporates by producing NH<sub>3</sub> and HCl; and then the reaction occurs at temperatures higher than 350 °C (i). By increasing temperature, gases pressure for forming both N<sub>2</sub> and H<sub>2</sub> are increased (ii). The silicon powders react with the HCl (iii) to form SiCl<sub>4</sub>. Consequently, the other chlorides, SiCl<sub>3</sub>, SiCl<sub>2</sub>, and SiCl form through the reaction with Silicon powder. Besides these reactions, the silicon reacts with the H<sub>2</sub> and Cl<sub>2</sub> and this reaction produces other two chlorides in the form of SiH<sub>2</sub>Cl<sub>2</sub> and SiHCl<sub>3</sub>. Finally, the H<sub>2</sub> and Cl<sub>2</sub> combine and produce the HCl gas. The vaporized compounds react with the etched surface of the base metal resulting in diffusion of the silicon. This allows for the formation of FeSi, FeSi<sub>2</sub> or Fe<sub>2</sub>Si.<sup>[28]</sup>

### 2. Plasma nitriding coating

Plasma nitriding on the surface of the steel evolves through four main reactions (11–14). The process schematic is shown can be described through Figure 1 [29]:



### B. Silicides Formation

The pack-siliconizing products formation and diffusion comprise four steps<sup>[28]</sup>: (i) halide activator is converted to the gas, (ii) the gas reacts with the elements of the coatings, (iii) reacted gas penetrates in the base metal, then creating the coated surface, and (iv) solid-state diffusion in the substrate.

At high temperature, Si reacts with the activators forming SiCl<sub>x</sub> and SiF<sub>y</sub> compounds. Then, gaseous chlorides and fluorides start to diffuse in the steel through the contact surface and the different formed phases.<sup>[30]</sup> Normally, the final coatings contain different layers of various compositions depending on the diffusion efficiency due to the time–temperature processing conditions.<sup>[27]</sup> The NH<sub>4</sub>Cl-activated pack cementation is very complex; it comprises various hydrogen-based compounds' formation such as SiH<sub>4-y</sub>Cl<sub>y</sub> (y=1-4).

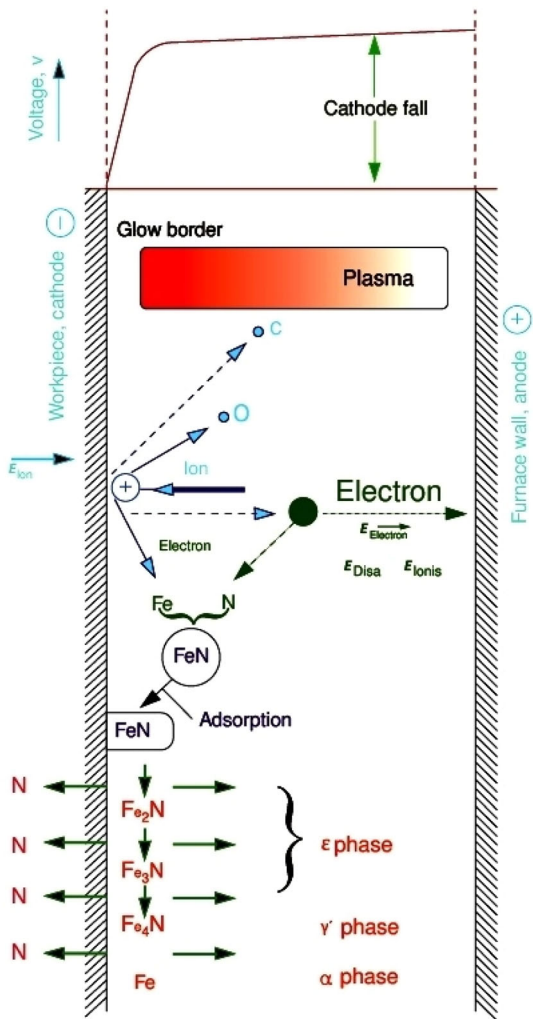


Fig. 1—The mechanisms of plasma nitriding.

Mainly the reacting species are recognized in  $\text{SiCl}_2$ ,  $\text{SiCl}_4$ ,  $\text{SiCl}_2\text{H}_2$ , and  $\text{SiCl}_3\text{H}$ .<sup>[30]</sup> Obviously, the coating thickness and its adhesion to the substrate are strongly related to the processing conditions employed during the deposition.

Microstructure of the coating observed by SEM on cross-section sample of the (HAPC) coatings formed at  $650^\circ\text{C}$  for 2 and 3 hours is shown in Figure 2. Given that the coatings form for all the powder compositions, the coatings thickness, measured from the SEM images, after 2 hours are 10, 9.2, and  $29\ \mu\text{m}$  for the powders no. 1, 2, and 3, the thickness of coating in 3 hours is 50, 76, and  $74\ \mu\text{m}$  for the powders no. 1, 2, and 3, respectively. By increasing the processing time and the percentages of activator and silicon, the diffusion of the silicon in the substrate increased. The chemical reactions evolution is related to the time, temperature, and the percentage of the activator. With increasing the activator percentage and treatment time, the chemical reactions velocity increases and consequently higher thickness can be obtained. The thickness of the coatings, for different composition and time, demonstrates that the diffusion of the silicon in the base metal significantly increases with

increasing the temperature and the halide percentage. As can be seen in Figure 2, the silicon has inter-diffusion in the base metal with different surface qualities.

In this case, those coatings produced with powders no. 2 and 3 show crack formation at the coating–substrate interface as well as inside the coating. Only the coating produced with the powder no. 1 appears with an acceptable adhesion and with the absence of cracks. The silicon diffusion was very low for the material treated at  $650^\circ\text{C}$  for 2 hours. On the other hand, silicon diffusion increases as the treatment time increases to 3 h. The diffusion is also largely improved by passing from 2 to 3 hours of heat treatment for the coatings produced with powders 2 and 3. The addition of NaF markedly improves the silicon penetration only for the powder no.2 leading to values close to those belonging to the coating produced with powder no.1.

Microstructure of the coating observed by SEM on cross-section sample of the coatings deposited through HAPC at the temperature of  $800^\circ\text{C}$  for 2 and 3 hours is shown in Figure 3.

By increasing temperature, the adhesion largely improves for all the employed powders. The coating thickness, deposited from the powder no.1 at 2 hours and powder no.2 at 3 hours, was detected to remarkably increase with temperature as shown in Figure 3. The achieved coating thicknesses, measured from the SEM images, at  $800^\circ\text{C}$  for powders 1, 2, and 3 in 2 hours were 47, 27, and  $24\ \mu\text{m}$ , respectively, and after 3 hours, the thicknesses were 41, 76, and  $32\ \mu\text{m}$ , respectively. The silicide coating thickness increased with increasing the percentage of the silicon inside the powder composition of the pack and with increasing the treatment time.

The diffusion behavior was also monitored through the Si profile along the coating thickness (Figures 4). As shown in Figures 3 and 4, the silicon diffusion increases as the silicon percentage in the powder and the treating time increase. The distribution of silicon increased from the base plate to the coating (Figure 4). Also, the EDS line scan provides the correct thickness of the silicon diffusion inside the substrate.

Finally, the HAPC process was performed at the highest temperature ( $950^\circ\text{C}$ ), and the SEM microstructure of the coatings are shown in Figure 5. Here, no cracks were observed for all the experienced processing conditions.

The coating thicknesses, measured from the SEM images, at  $950^\circ\text{C}$  for powders no.1, 2, and 3 in 2 hours were 79, 83, and  $92\ \mu\text{m}$ , respectively, and after 3 hours, the thicknesses were 89, 356, and  $356\ \mu\text{m}$ , respectively. Also, the same thickness of the coating is shown for the pack composition no.3 with the holding time of the 3 hours by Najafzadeh *et al.*<sup>[31]</sup> The coatings, produced by adding the NaF as an activator, show increased thickness due to the silicon diffusion which largely improved thanks to the increased activation energy. This behavior is observed for all the treating times at the temperature of  $950^\circ\text{C}$ . The thickness of the silicide coating is related to the alloying elements, time, and temperature.<sup>[32]</sup> The best conditions to obtain coatings with high thickness without cracking are those deposited at  $950^\circ\text{C}$  and 3 hours. The mean reasons for enhancing



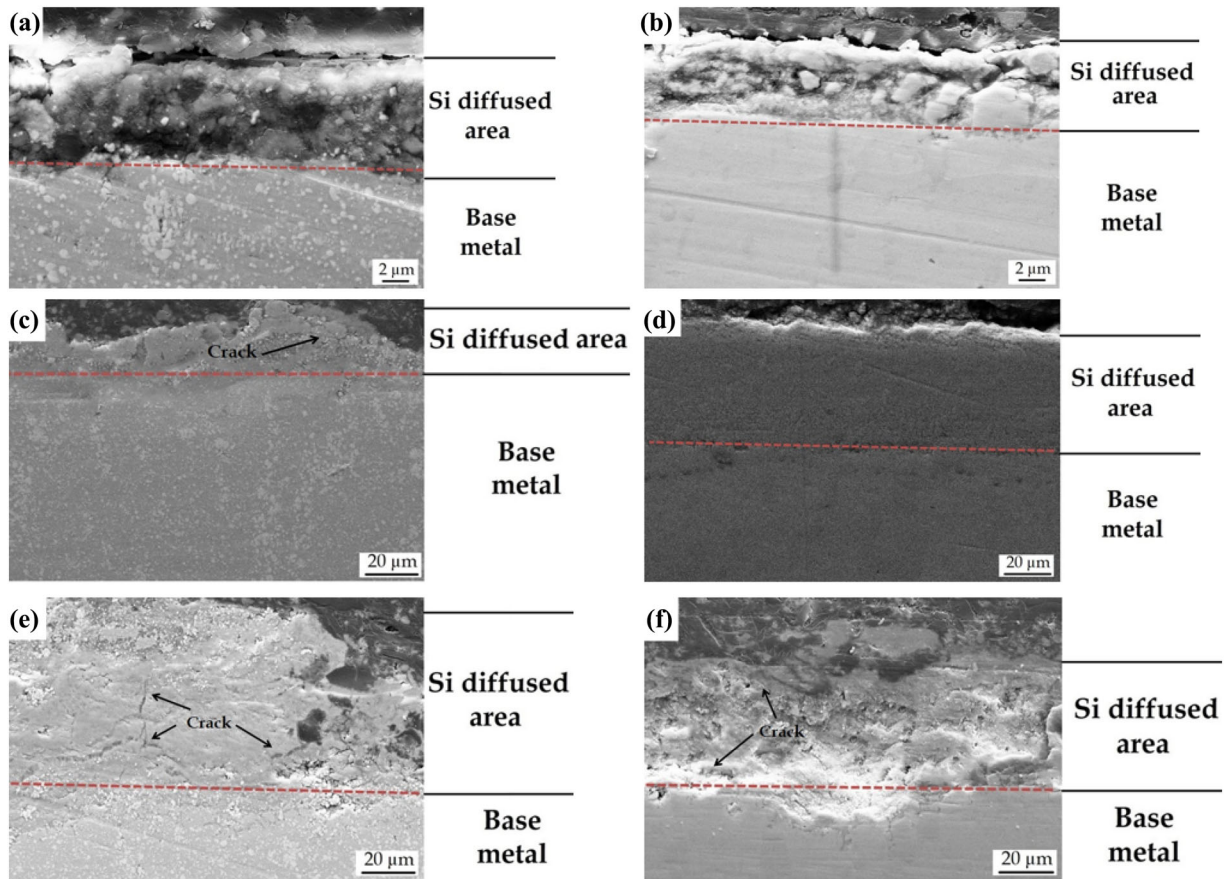


Fig. 2—Microstructure of the coating observed by SEM on cross-section sample of the HAPC coatings formed at 650 °C for (a) 12, (b) 22, (c) 32, (d) 13, (e) 23, and (f) 33.

the thickness of the silicide coating with the augmenting temperature from 650, 800, and 950°C are recognized in the halide vapors easy formation as the temperature increases. This is the main contribution to the thickness enhancement.

The powder compositions no.1 and no.2 deposited at 950°C and 3 hours were selected for plasma-nitriding treatment. Those coatings will be indicated in the following as HAPC 1 and HAPC 2, respectively. Their hardness profiles, before the plasma-nitriding process, are shown in Figure 6(a). For comparison, the Si profile along the thickness is shown in Figure 6(b). The silicon coating substantially shows increases in the hardness.<sup>[33]</sup>

### C. Nitriding

The nitriding of the steel is related to the different parameters such as the composition of the alloy, the mixture of the nitrogen and hydrogen, and treating temperature and time.<sup>[34,35]</sup> Obviously, in the present case, the nitriding evolution and the consequent phases formation mainly depend on the silicon-rich material and silicides precipitated on the steel surface during the previous coating process. Microstructure of the coating observed by SEM on cross-section sample of the HAPC 1 and 2 coatings after plasma nitriding is shown in Figure 7. The average

thickness of the  $\text{Si}_3\text{N}_4$  coating as shown in Figure 7 for HAPC 1 is 37  $\mu\text{m}$  and HAPC 2 is 115  $\mu\text{m}$ , respectively.

The EDS analyses results of the HAPC 1 and HAPC 2 coatings are summarized in Figure 8. The compositional profiles show that the HAPC 2 coating has higher percentage of Si and N than the HAPC 1. Habibollahzadeh et al. used the EDS analyses for the recognizing the N and the other elements on the coating.<sup>[36]</sup> As previously mentioned, the huge amount of Si along the nitrogen diffusion path will influence the precipitates formation and composition. In fact, although the nitrogen quantity is common for a traditional nitriding process, the silicon quantity belonging to the previous treatment is very high.

The kinetic and thermodynamic reactions, leading to the coatings formation, are due to the diffusion in the substrate. So, the diffusion path of silicon and its compounds formation are fundamental for the analysis of the coatings properties and stability.<sup>[32]</sup>

The XRD analysis allows identifying the different phases forming during the process. The XRD pattern of the siliconizing coating is shown in Figure 9(a). The XRD analysis performed on the surface of the silicon coating indicated the three phases: FeSi<sub>2</sub>, FeSi, and Fe<sub>2</sub>Si. The same FeSi intermetallics are founding by Najafizadeh et al.<sup>[37]</sup> The XRD pattern of the

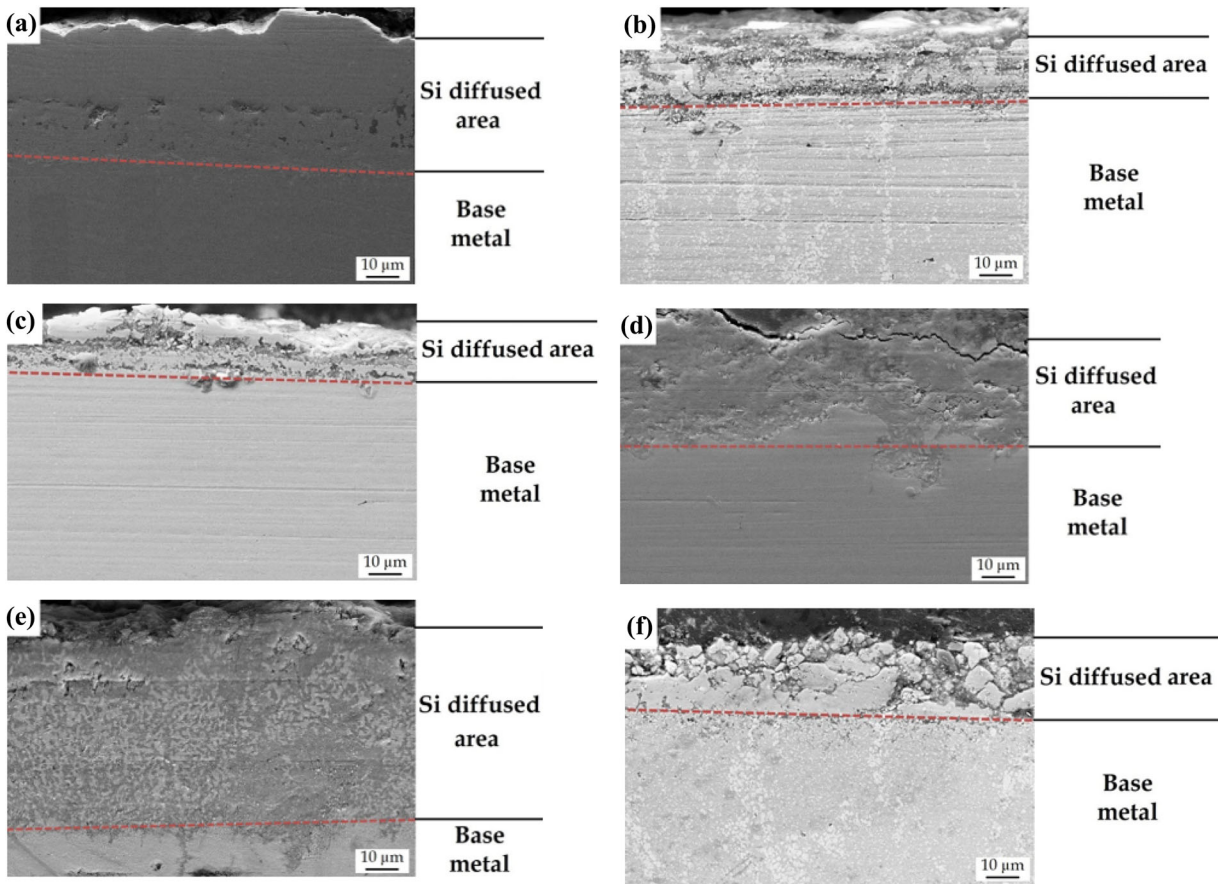


Fig. 3—Microstructure of the coating observed by SEM on cross-section sample of the HAPC coatings performed at 800 °C for (a) 12, (b) 22, (c) 32, (d) 13, (e) 23, and (f) 33.

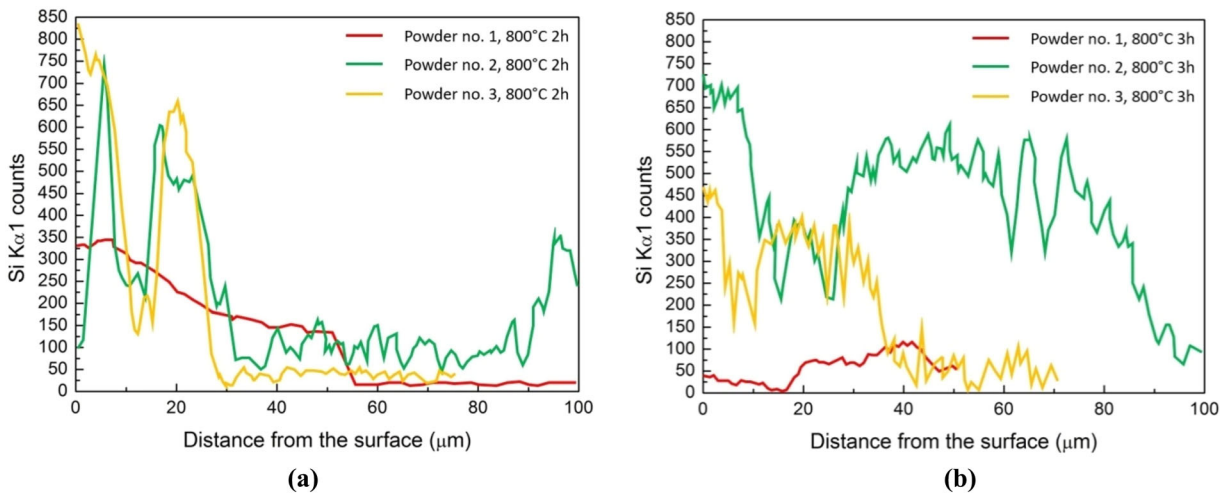


Fig. 4—SEM-EDS Linear analysis of the silicon in the steel coated at 800 °C for (a) 2 h and (b) 3 h.

plasma-nitrided HAPC 1 coating is shown in Figure 9(b). The results show the  $\gamma$  phase formation during silicon nitriding.<sup>[38]</sup> According to the XRD pattern, the main reinforcing phases were  $\gamma$ - $\text{Si}_3\text{N}_4$  (cubic),  $\text{Fe}_3\text{N}$  (hexagonal),  $\text{Fe}_4\text{N}$  (cubic),  $\text{CrN}$  (cubic), and  $\text{CrSiAl}$  (hexagonal). The XRD pattern of the plasma-nitrided HAPC 2 coating is shown in

Figure 9(c). The results show the formation of the  $\beta$  phase.<sup>[39]</sup> According to the XRD pattern of the HAPC 2, the  $\beta$ - $\text{Si}_3\text{N}_4$  (hexagonal) and other phases such as  $\text{Fe}_4\text{N}$  (cubic),  $\text{CrFe}$  (cubic),  $\text{CrFeSi}$  (hexagonal),  $\text{N}_2\text{OSi}_2$ , and  $\text{Fe}_2\text{N}$  (orthorhombic) were detected. The detection of the different compounds precipitation is

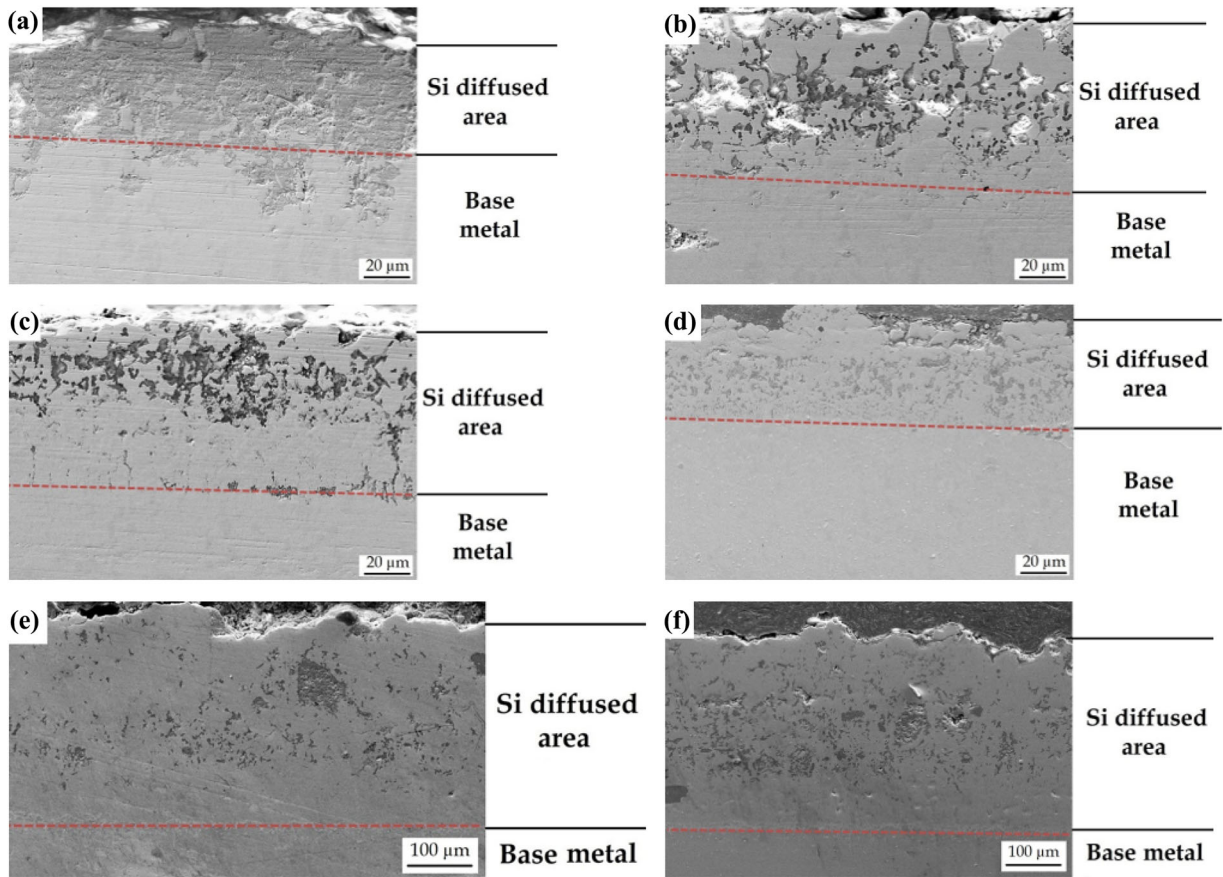


Fig. 5—Microstructure of the coating observed by SEM on cross-section sample of the HAPC coatings performed at 950 °C for (a) 12, (b) 22, (c) 32, (d) 13, (e) 23, and (f) 33.

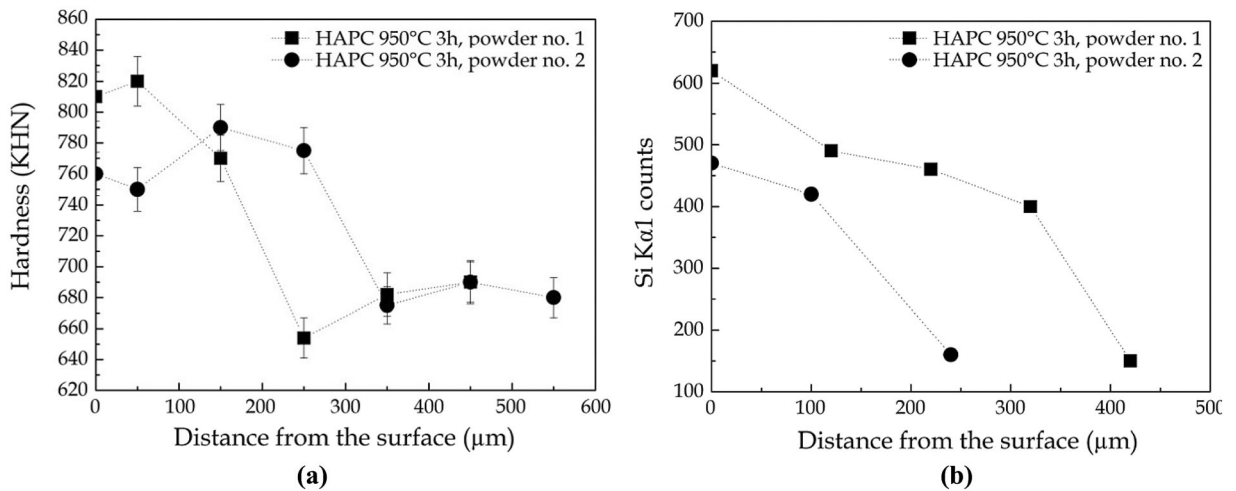


Fig. 6—(a) Hardness profiles of the AISI D2 steel after coating through HAPC at 950 °C for 3 hours by employing powders of compositions 1 and 2; (b) Si profile along the coating thickness for both the powders.

fundamental because brittleness can be induced in the material if precipitates evolve in an undesired way.<sup>[40]</sup>

The hardness profiles after plasma nitriding are shown in Figure 10. The maximum hardness of the plasma-nitrided coating on HAPC 1 sample appears marginally higher than the hardness of the HAPC 2

coating one. This is attributed to the different phases evaluation during the nitriding process. The hardness of the  $\gamma$ - $\text{Si}_3\text{N}_4$  phase<sup>[41]</sup> is higher than the  $\beta$ - $\text{Si}_3\text{N}_4$ .<sup>[42]</sup>

For comparison, plasma nitriding was performed on the steel without HAPC treatment, the phases evolution spectrum is shown in Figure 11. According to the XRD



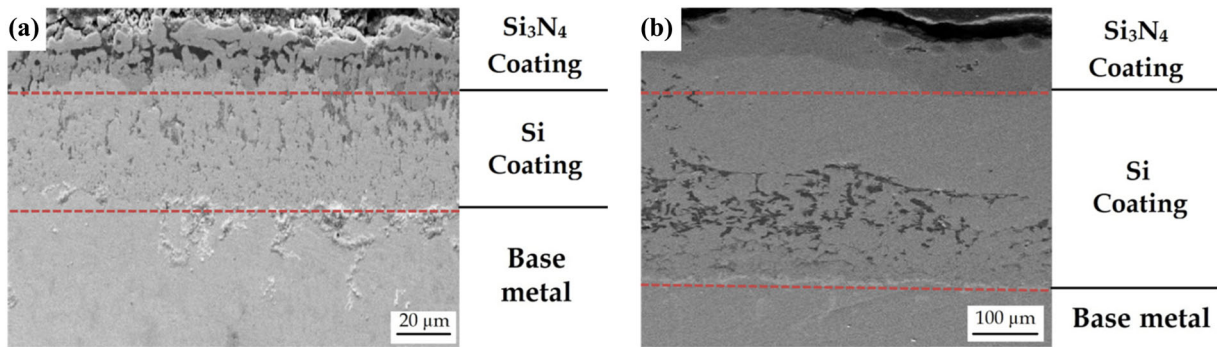


Fig. 7—Microstructure of the coating observed by SEM on cross section of the siliconized coating after plasma nitriding (a) HAPC 1 and (b) HAPC 2.

pattern of the D2 tool steel after plasma nitriding, the  $\text{Fe}_4\text{N}$  and  $\text{Fe}_3\text{N}$  phases are detected on the surface of the AISI D2 steel.

The main-hardening precipitates were  $\epsilon\text{-Fe}_3\text{N}$  and  $\gamma'\text{-Fe}_4\text{N}$ .  $\gamma'\text{-Fe}_4\text{N}$  which were recognized as the main phases, and these are also very efficient in improving the wear resistance of the steel.<sup>[43]</sup> As a consequence, it is expected that the precipitate states can lead to different wear behaviors.<sup>[43–45]</sup> By increasing the percentage of the nitrogen in the gas during plasma nitriding, roughness of the surface increased.<sup>[46]</sup>

#### D. Wear Behavior

The weight loss after sliding clearly shows that the wear resistance of the steel increases through coating operations (Figure 12). The wear resistance increases with sliding distance. The friction coefficient variation during sliding is shown in Figure 13 for all the studied coatings.

First of all, the initial variation of the friction coefficient depends on the surface roughness differences due to the various surface treatments. Then the friction coefficient varies for the different coating types because of the intrinsic mechanical properties of the coated layers as will be precisely described through the nano-indentation behavior of the studied materials.

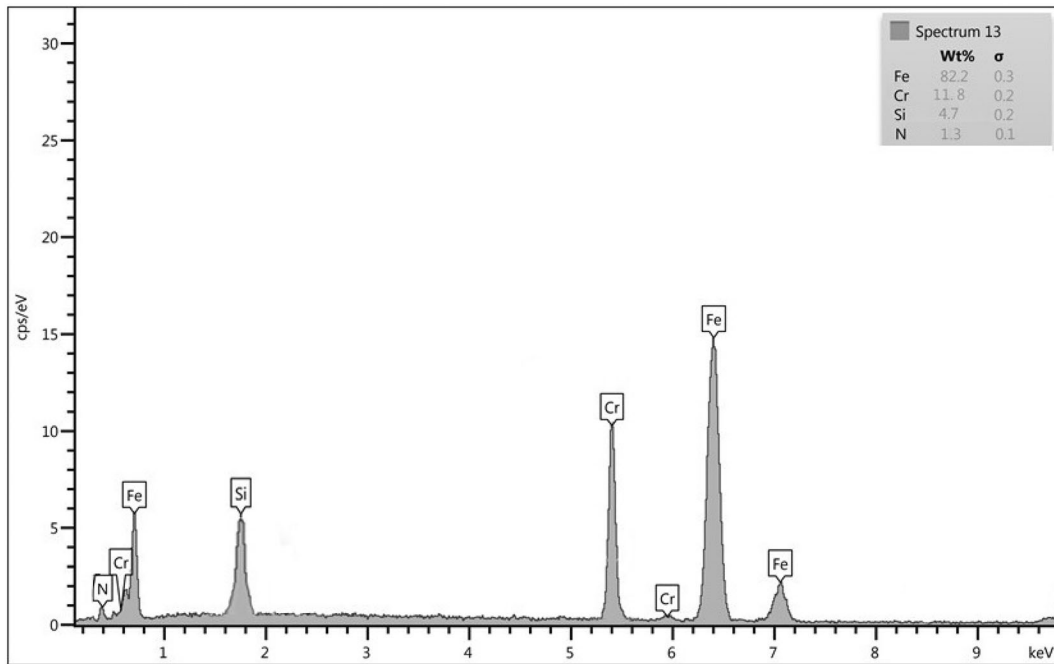
Plasma-nitrided HAPC 1 sample shows the best performances in all the conditions. Plasma nitriding without HAPC shows a higher wear resistance with respect to the nitrided HAPC 2 sample up to a sliding distance of 200 meters. The plasma-nitrided sample weight loss is higher also with respect to the HAPC 1. This confirms the brittleness of the coating performed by employing NaF as activation compound during HAPC. This behavior was explained as dependent on the precipitation state of the steel belonging to the different coating sequences.<sup>[47,48]</sup> Plasma-nitrided AISI D2 steel shows a good wear resistance due to the optimal precipitates mainly recognized in  $\gamma'\text{-Fe}_4\text{N}$ , this is reported to be very effective to improve the wear properties.<sup>[49,50]</sup> The HAPC 1+ plasma-nitriding coating is shown to have higher wear resistance due to the huge precipitation of hard  $\text{Si}_3\text{N}_4$  silicides. These silicides result excellent for the further increase in wear resistance

and are responsible for the remarkable decrease of the friction coefficient (Figure 13, the fitting curve for the friction coefficient is shown in red). In the case of the HAPC 2+ plasma nitriding, the presence of brittle nitrogen silicon dioxide phases leads to a decrease in the wear resistance (lower than the plasma nitride steel). Here, as a partial conclusion, even if the addition of NaF as activator is very effective in realizing very thick siliconized coatings; those coatings produced with the sole  $\text{NH}_4\text{Cl}$  activator show improved mechanical properties after plasma nitriding.

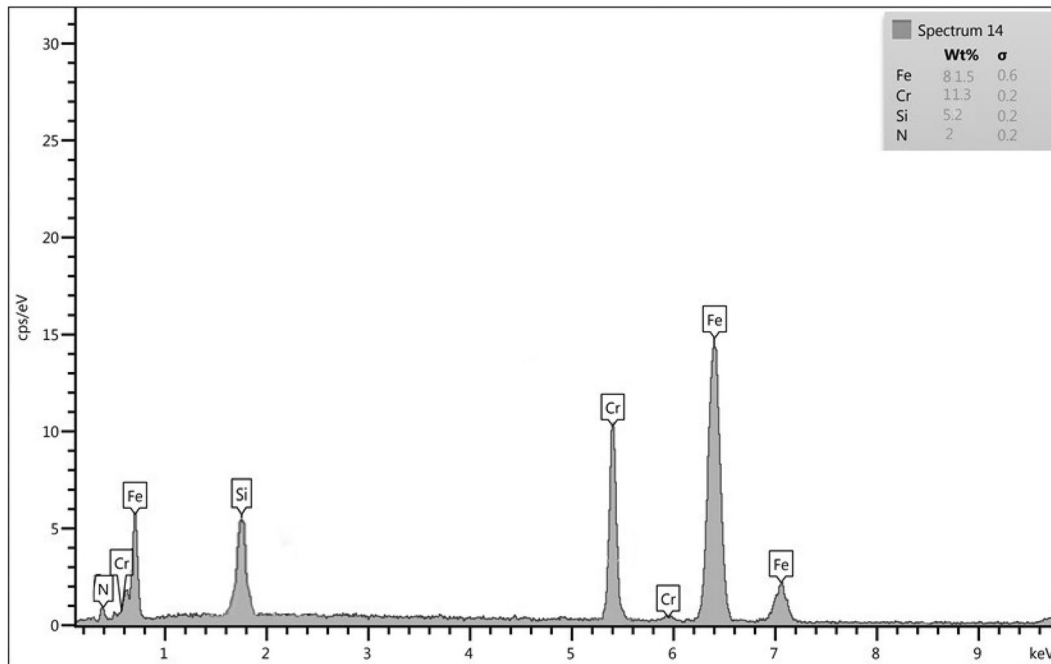
The plasma nitride sample shows a slight increase of the friction coefficient for low sliding distance, and then it decreases up to the plateau value. A similar behavior with lower friction coefficient is shown for the HAPC 2+ plasma-nitriding coating. The HAPC 1+ plasma-nitriding coating shows lower friction coefficient with an almost constant behavior as a function of the sliding distance. In order to further investigate such behavior, nano-indentation tests were performed on the base AISI steel and on the nitride coatings in both the studied conditions. The results are shown in Figure 14.

As a matter of fact, the nano-indentation results give a clear explanation of the wear behavior of the coatings. In fact, the plasticity index largely increases for HAPC2+ plasma nitriding and HAPC1+ plasma nitriding with respect to the AISI D2 steel. The precipitation behavior leads to strong modifications in the elastic behavior as well as in the material hardness. Obviously, this acts with different rates as a function of the various treatments. Here, the proportion between hardness (H) and elastic modulus (E), known as plasticity index, is a very suitable parameter to evaluate the wear behavior of coatings. The optimization of wear resistance was measured with by plasticity index for specifying the extent of elastic behavior in surface contact.<sup>[51]</sup> In particular, the elastic strain to failure (depending on the H/E proportion) is considered an applicable parameter to support the wear resistance instead using only hardness for measuring wear resistance. In particular, the higher the plasticity index is, the best the friction coefficient results demonstrating the best stability of the coatings due to the precipitation state induced by the surface treatments. So as a partial conclusion, the huge precipitation due to HACP





(a)

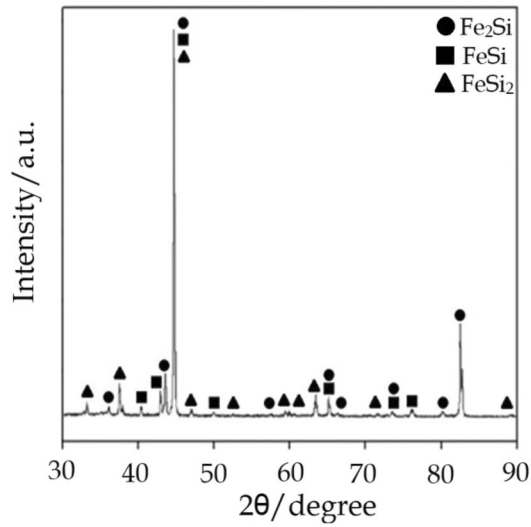


(b)

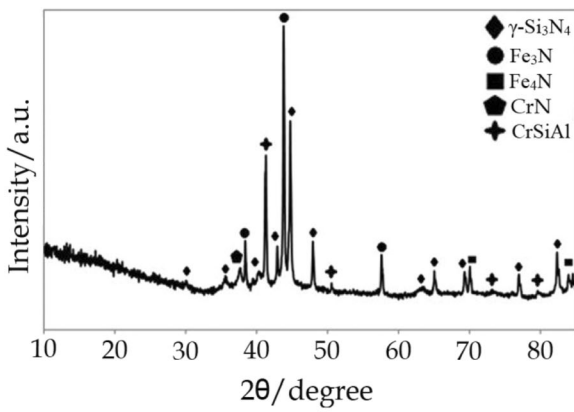
Fig. 8—The SEM-EDS point of the (a) HAPC 1 + plasma nitriding and (b) HAPC 2 + plasma nitriding.

and plasma nitriding leads to high hardness and high elastic modulus leading to a wear resistance and stable surface.

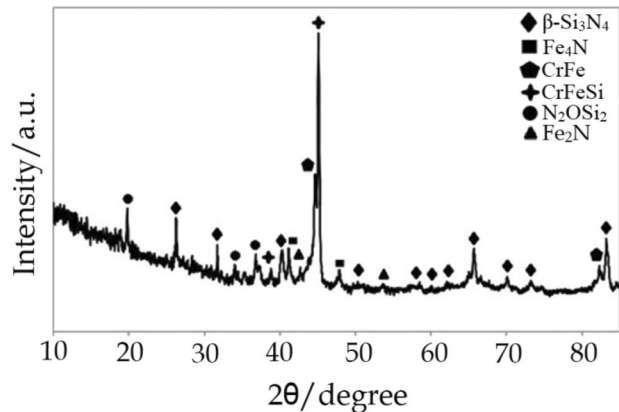
Generally, the higher the H/E ratio is, the higher the wear properties are expected.<sup>[52,53]</sup> With this behavior, the plasticity index (Hardness/Elastic modulus) varies



(a)



(b)



(c)

Fig. 9—X-ray diffraction pattern of (a) the siliconizing from HAPC 2 coating, (b) the plasma-nitriding HAPC 1 coating, (c) the plasma-nitriding HAPC 2 coating.

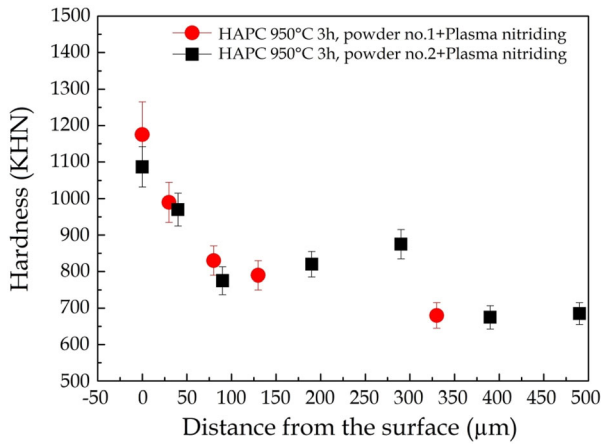


Fig. 10—Micro-hardness depth profile of the siliconized samples after plasma nitriding.

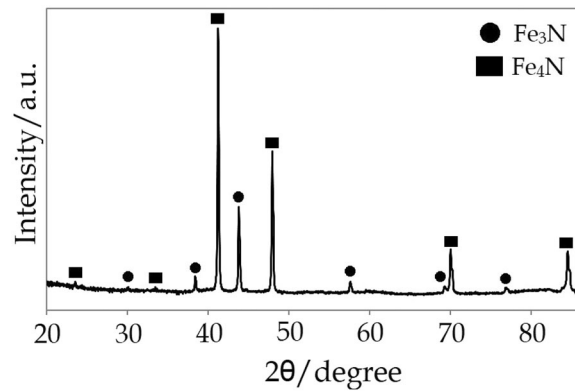


Fig. 11—XRD pattern of the AISI D2 steel after plasma nitriding.

from 0.051 to 0.06, being perfectly consistent with the different wear behaviors observed during sliding.

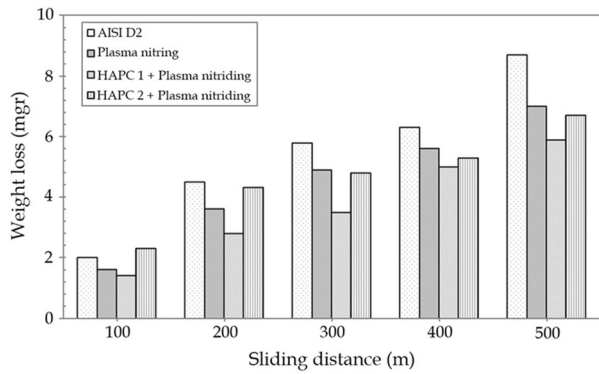
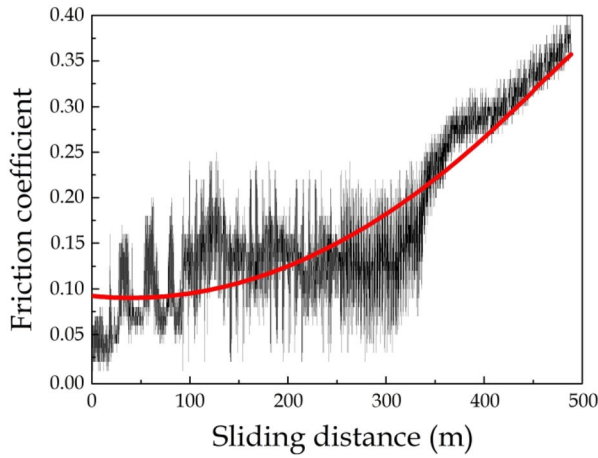
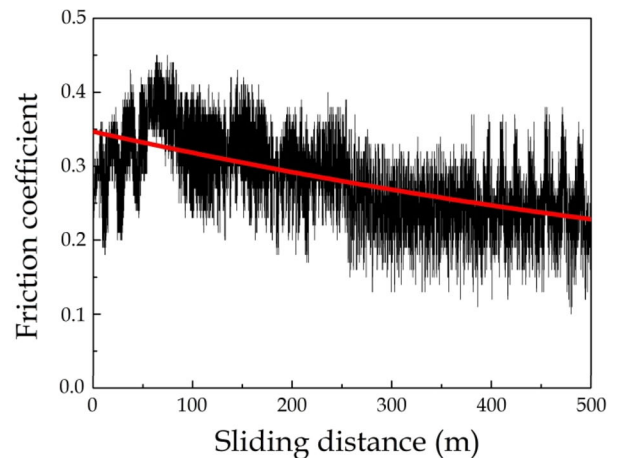


Fig. 12—Variation of weight loss with the sliding distance after pin on disk tests.

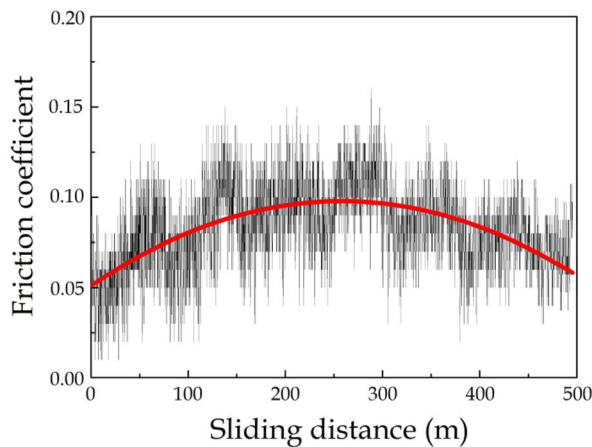
The morphology of the worn surface was examined allowing to identify the wear mechanisms acting during sliding. The SEM images of the specimens are shown in Figures 15(a) through (d), after the wear test at 30N load with the 0.5m/s. The SEM microstructure of AISI D2 in the as-received condition and after plasma nitriding is shown in Figures 15(a) and (b), respectively. The morphologies of the worn surface show large plastic deformation, the particles of material emerge, and also adhesion wear can be underlined. The main wear mechanism is adhesive. In this case, there is an adhesion between pin and disk material without using lubricant. The SEM microstructure after silicon nitriding is shown in Figures 15(c) and (d). The wear grooves are revealed by the observation of micro-pores on this coating. As can be seen from Figure 7, the continual plastic deformation of the coating and particles emerge cause to form the micro-pores on the surface.<sup>[54]</sup> The other reasons for the formation of the micro-pores are releasing and entrapment phenomena of nitrogen within the superficial oxide layer.<sup>[55]</sup>



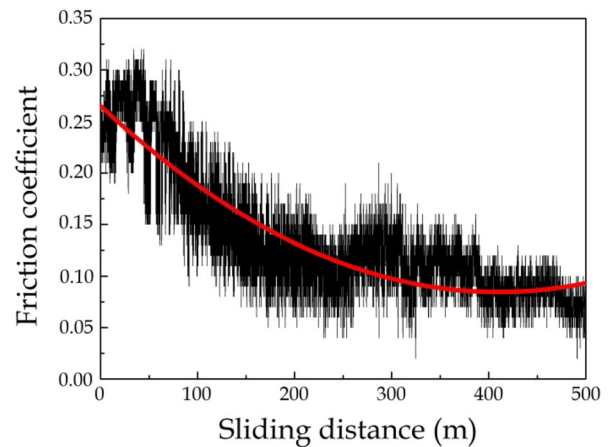
(a)



(b)



(c)



(d)

Fig. 13—Friction coefficient as a function of the sliding distance (a) AISI D2, (b) plasma nitriding, (c) HAPC 1 + plasma nitriding, and (d) HAPC 2 + plasma nitriding.



#### IV. CONCLUSIONS

In the current study, silicide coatings were deposited through halide activated pack cementation by employing different siliconizing powder compositions. The concluding remarks are

1. Silicon diffusion increases as the treating temperature increases from 650 to 950 °C.

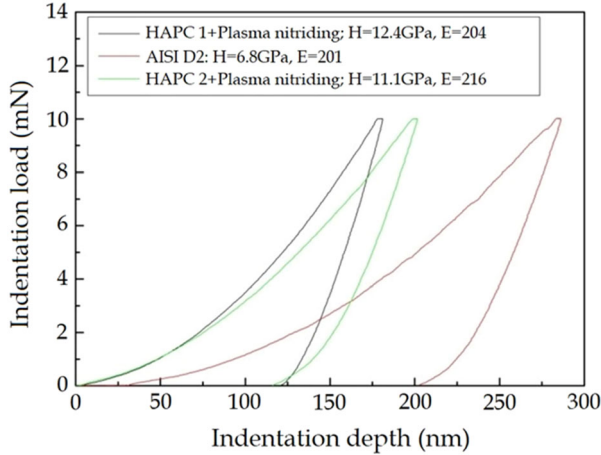


Fig. 14—Indentation curves for the plasma-nitrided coatings.

2. The optimal combination for having better thickness occurred using temperature of 950 °C and treating time of 3 hours.
3. By adding NaF to  $\text{NH}_4\text{Cl}$  as an activator, the thickness is far higher with respect to the treating condition employing only  $\text{NH}_4\text{Cl}$ .
4. By employing  $\text{NH}_4\text{Cl}$  or  $\text{NH}_4\text{Cl} + \text{NaF}$  as activators, a remarkable modification of phases formation was revealed.
5. The plasma-nitriding coating belonging to the  $\text{NH}_4\text{Cl}$ -siliconized steel showed the most hardened precipitated such as  $\gamma\text{-Si}_3\text{N}_4$  leading to higher hardness and wear resistance.
6. By using  $\text{NH}_4\text{Cl} + \text{NaF}$ , the  $\beta\text{-Si}_3\text{N}_4$  phase was found, which plays a key role in wear resistance but due to oxidation  $\text{N}_2\text{OSi}_2$ , the wear resistance is decreased and then increased in comparison to the as nitrided steel.
7. The mechanical behavior of the plasma nitriding coating belonging to the  $\text{NH}_4\text{Cl}$ -siliconized steel, analyzed through nano-indentation, revealed that the precipitation state leads to a significant increase in the plasticity index confirming the improved wear properties.
8. By increasing sliding distance, wear resistance increased significantly. In the presence of  $\text{Si}_3\text{N}_4$ , the friction coefficient decreased.

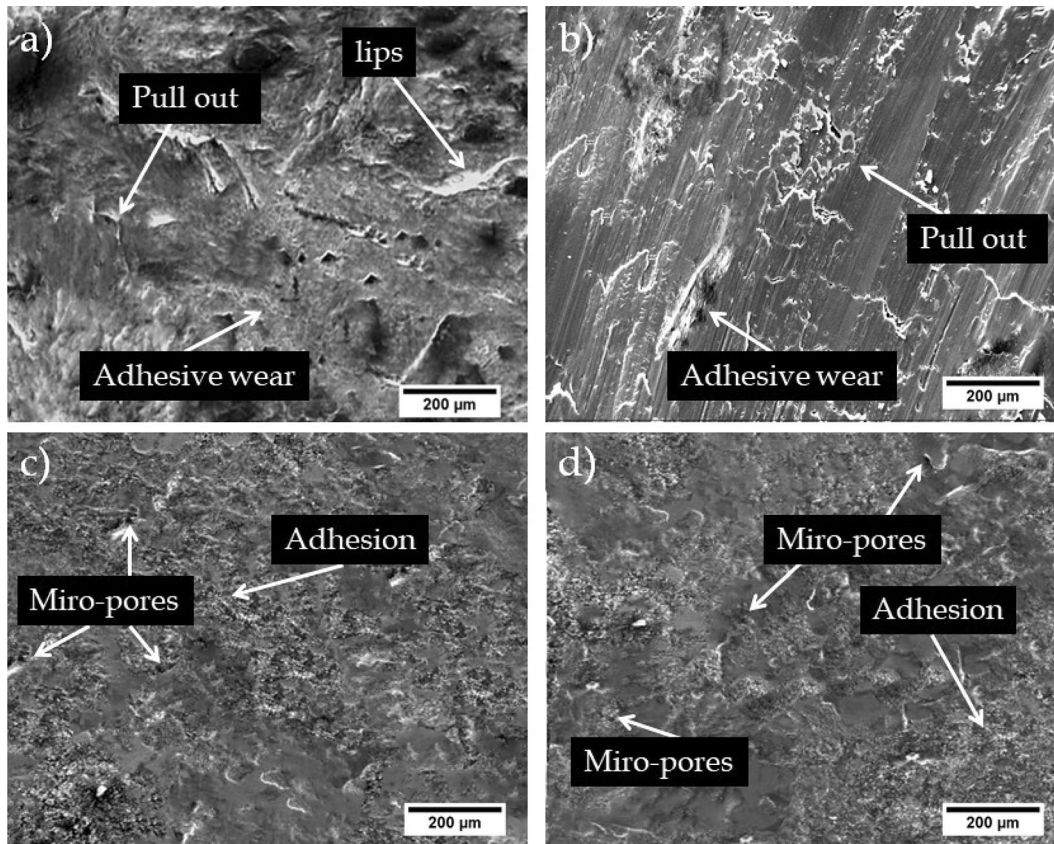


Fig. 15—SEM images of the worn surface of the (a) AISI D2, (b) plasma nitriding, (c) HAPC 1 + plasma nitriding, and (d) HAPC 2 + plasma nitriding.

## FUNDING

Open access funding provided by Università del Salento within the CRUI-CARE Agreement.

## CONFLICT OF INTEREST

The authors declare they have no conflict of interest.

## OPEN ACCESS

This article is licensed under a Creative Commons Attribution 4.0 International License, which permits use, sharing, adaptation, distribution and reproduction in any medium or format, as long as you give appropriate credit to the original author(s) and the source, provide a link to the Creative Commons licence, and indicate if changes were made. The images or other third party material in this article are included in the article's Creative Commons licence, unless indicated otherwise in a credit line to the material. If material is not included in the article's Creative Commons licence and your intended use is not permitted by statutory regulation or exceeds the permitted use, you will need to obtain permission directly from the copyright holder. To view a copy of this licence, visit <http://creativecommons.org/licenses/by/4.0/>.

## REFERENCES

1. W.H. Wills: *Trans. ASM*, 1935, vol. 23, p. 469.
2. S.J. Gobbi, V.J. Gobbi, G. Reinke, P.V. Muterle, and D.M. Rosa: *Mater. Sci. Technol.*, 2019, vol. 35 (11), pp. 1355–64.
3. A.M. Khan, M. Jamil, A. Ul Haq, S. Hussain, L. Meng, and N. He: *Ind. Lubr. Tribol.*, 2019, vol. 71 (2), pp. 267–77.
4. D. Bombač, M. Terčelj, G. Kugler, and I. Peruš: *Mater. Sci. Technol.*, 2018, vol. 34 (14), pp. 1723–36.
5. A. Yapici, S.E. Aydin, V. Koc, E. Kanca, and M. Yildiz: *Prot. Met. Phys. Chem. Surf.*, 2019, vol. 55 (2), pp. 341–51.
6. M. Keddad and M. Kulka: *Phys. Met. Metall.*, 2018, vol. 119 (9), pp. 842–51.
7. J. Xiang, F. Xie, X. Wu, and Y. Yu: *Tribol. Int.*, 2019, vol. 136, pp. 45–57.
8. J. Tian, W.H. Yu, W. Tian, J. Zhao, Y.Q. Li, and Y.Z. Liu: *Surf. Eng.*, 2015, vol. 31 (4), pp. 289–94.
9. X.J. Lu and Z.D. Xiang: *Met. Trans.*, 2017, vol. A48, pp. 580–83.
10. J. Sun, T. Li, G.-P. Zhang, and Q.-G. Fu: *J. Alloys Compd.*, 2019, vol. 790, pp. 1014–22.
11. W.L. Byeong: *Int. J. Mod. Phys.*, 2018, vol. B 32, p. 1840056.
12. N. Chaia, L. Portebois, S. Mathieu, N. David, and M. Vilasi: *J. Nucl. Mater.*, 2017, vol. 484, pp. 148–56.
13. X. Li, G. Hu, J. Tian, W. Tian, W. Xie, and X. Li: *J. Mater. Eng. Perform.*, 2018, vol. 27, pp. 1073–82.
14. X. Li, X. Guo, and Y. Qiao: *Trans. Nonferrous Met. Soc. China*, 2016, vol. 26, pp. 1892–1901.
15. J. Xiao, Y. Huang, Q. Zhou, J. Wang, and X. He: *Surf. Eng.*, 2019, vol. 35 (8), pp. 719–27.
16. Z.A. Fazel, H. Elmkhah, M. Nouri, and A. Fattah-Alhosseini: *Mater. Res. Express*, 2019, vol. 6 (5), p. 412.
17. J. Xue, G. Tao, C. Tang, N. Xu, F. Li, and C. Yin: *Surf. Coat. Technol.*, 2020, vol. 382, p. 125217.
18. C.-B. Tang, F.-R. Wen, H.-X. Chen, J.-J. Liu, G.-Y. Tao, X. Ni-jun, and J.-Q. Xue: *J. Alloys Compd.*, 2019, vol. 778, pp. 972–81.
19. I. Ebrahimzadeh and F. Ashrafzadeh: *Ceram. Int.*, 2014, vol. 40 (10), pp. 16429–39.
20. F. Haftlang, A. Habibolahzadeh, and M. Heydarzade Shohi: *Vacuum*, 2014, vol. 107, pp. 155–58.
21. L. Mouri, I. Mabile, C. Fiaud, J. Amouroux, G. Catillon, and R. Gras: *Thin Solid Films*, 2001, vol. 389 (1), pp. 153–60.
22. I. Asemphah, J. Xu, L. Yu, H. Ju, F. Wu, and H. Luo: *Surf. Eng.*, 2019, vol. 35 (8), pp. 701–709.
23. D. Stathokostopoulos, D. Chaliampalias, N. Pliatsikas, S. Kassavetis, E. Pavlidou, P. Patsalas, S. Logothetidis, K. Chrissafis, and G. Vourlias: *Surf. Eng.*, 2018, vol. 34 (3), pp. 243–50.
24. S. Semboshi, S. Kimura, A. Iwase, and N. Ohtsu: *Surf. Coat. Technol.*, 2014, vol. 258, pp. 691–98.
25. J. Ikeda, S. Semboshi, A. Iwase, W. Gao, and A. Sugawara: *Metall. Mater. Trans.*, 2015, vol. 56 (3), pp. 297–302.
26. D. Ueyama, S. Semboshi, Y. Saitoh, N. Ishikawa, K. Nishida, N. Soneda, F. Hori, and A. Iwase: *Japan J. Appl. Phys.*, 2014, vol. 53 (5S1), p. 05FC04.
27. J.H. Perepezko, T.A. Sossaman, and M. Taylor: *J. Therm. Spray Technol.*, 2017, vol. 26 (5), pp. 929–40.
28. S.P. Chakraborty, S. Banerjee, I.G. Sharma, and A.K. Suri: *J. Nucl. Mater.*, 2010, vol. 403, pp. 152–59.
29. D. Pye: *Practical Nitriding and Ferritic Nitro-Carburizing*, 1st ed., ASM International Technical Book, Ohio, 2003, pp. 78–79.
30. Z.D. Xiang and P.K. Datta: *Mater. Sci. Eng. A*, 2003, vol. 356, pp. 136–44.
31. M. Najafzadeh and M. Ghasempour-Mouziraji: *Silicon*, 2020, vol. 13, pp. 2233–42.
32. Y.A. Balandin and A.S. Kolpakov: *Met. Sci. Heat Treat.*, 2006, vol. 48, pp. 127–30.
33. L. Huang, X. Wu, F. Xie et al.: *J. Wuhan Technol. Mater. Sci. Ed.*, 2017, vol. 32, pp. 245–49.
34. P. Cavaliere, A. Perrone, and A. Silvello: *J. Comput. Des. Eng.*, 2016, vol. 3, pp. 71–90.
35. P. Cavaliere, G. Zavarise, and M. Perillo: *Comput. Mater. Sci.*, 2009, vol. 46, pp. 26–35.
36. A. Habibolahzadeh and F. Haftlang: *Mater. Res. Express*, 2019, vol. 6, p. 096444.
37. M. Najafzadeh, M. Ghasempour-Mouziraji, and D. Zhang: *Silicon*, 2021, <https://doi.org/10.1007/s12633-021-01057-9>.
38. J.Z. Jiang, K. Ståhl, R.W. Berg, D.J. Frost, T.J. Zhou, and P.X. Shi: *Europhys. Lett. EPL*, 2000, vol. 51 (1), pp. 62–67.
39. T. Nishimura, X. Xu, K. Kimoto, N. Hirotsaki, and H. Tanaka: *Sci. Technol. Adv. Mater.*, 2007, vol. 8 (7–8), p. 635.
40. F. Xie, S. Xu, and J. Pan: *Mater. Perf. Charact.*, 2018, vol. 7 (5), pp. 1164–77.
41. J.Z. Jiang, F. Kragh, D.J. Frost, K. Ståhl, and H. Lindelov: *J. Phys. Condens. Matter.*, 2001, vol. 13 (22), p. 515.
42. M. Nakamura, K. Hirao, Y. Yamauchi, and S. Kanzaki: *Wear*, 2003, vol. 254, pp. 94–102.
43. T. Liapina, A. Leineweber, and E.J. Mittemeikier: *Scr. Mater.*, 2003, vol. 48, pp. 1643–48.
44. D. Singh, A.M. Gatey, R.S. Devan, V. Antunes, F. Alvarez, C.A. Figueroa, A.A. Joshi, and S.S. Hosmani: *Surf. Eng.*, 2019, vol. 35 (3), pp. 205–15.
45. Y. Yang, J.H. Guo, M.F. Yan, Y.D. Zhu, Y.X. Zhang, and Y.X. Wang: *Surf. Eng.*, 2018, vol. 34 (2), pp. 132–38.
46. F. Ashrafzadeh: *Surf. Coat. Technol.*, 2003, vols. 174–175, pp. 1196–1200.
47. B. Podgornik, B. Zuzek, F. Kafexhiu, and V. Leskovšek: *Tribol. Lett.*, 2016, vol. 63, p. 147.
48. J. Pribbenow, M. Mejauschek, P. Landgraf, G. Braüer, and T. Lampke: *IOP Conf. Ser. Mater. Sci. Eng.*, 2019, vol. 480 (1), p. 01209.
49. T.V. Doan, D. Kusmič, M. Pospichal, and D. Dobroćký: *IOP Conf. Ser. Mater. Sci. Eng.*, 2017, vol. 179 (1), p. 012017.
50. T. Van Doan, D. Kusmič, M. Pospichal, Q.D. Tran, and V.T. Nguyen: *Manuf. Technol.*, 2017, vol. 17 (2), pp. 168–74.
51. S.R. Anvari, S.M. Monirvaghefi, and M.H. Enayati: *Surf. Eng.*, 2015, vol. 31 (9), pp. 693–700.
52. A. Matthews, and A. Leyland, Materials related aspects of nanostructured tribological coatings, In: Martinu L, Bardos L, Shimshock R, editors. Proceedings of the 51st Annual Technology Conference on Society of vacuum coaters. Albuquerque, CO, 2008, pp. 40–45.

53. W. Ni, Y.T. Cheng, M.J. Lukitsch, A.M. Weiner, L.C. Lev, and D.S. Grummon: *Appl. Phys. Lett.*, 2004, vol. 85, pp. 4028–30.
54. M. Naeem, H.A. Raza, M. Shafiq, M. Zaka-ul-Islam, J. Iqbal, J.C. Díaz-Guillén, and M. Zakaullah: *Mater. Res. Express*, 2017, vol. 4, p. 1107.

55. I. Milosev, H.H. Strehblow, and B. Navinsek: *Surf. Coat. Technol.*, 1995, vols. 74–75, pp. 897–902.

**Publisher's Note** Springer Nature remains neutral with regard to jurisdictional claims in published maps and institutional affiliations.